Progress in Physics of Applied Materials 5 (2025), 73 – 82

Semnan University

Progress in Physics of Applied Materials

journal homepage: https://ppam.semnan.ac.ir/

Structural, Electronic, and Magnetic Properties of $Mn_2NbAl_{1-x}Si_x$ (x=0.0–1.0) Alloys

Seyyed Mojtaba Alavisadr (Zareii) [a*]

[a] *Department of Basic Sciences, Birjand University of Technology, Birjand, Iran*

ARTICLE INFO

Article history:
Received: 16 February 2025
Revised: 9 June 2025
Accepted: 11 June 2025
Published online: 4 July 2025

Keywords:
Magnetic Intermetallic;
Density Functional Theory;
Electronic Structure;
Half-Metallic.

ABSTRACT

The structural, electronic, and magnetic properties of the novel $Mn_2NbAl_{1-x}Si_x$ (x=0.0–1.0) alloys were surveyed by using the density functional theory. The formation and cohesive energy results confirm that all members of these series are thermodynamically stable, but the Hg_2CuTi-type structure has lower stability compared to the Cu_2MnAl-type structure. The results also reveal that with increment of Si content, the lattice constant decreases linearly from 6.01 to 5.88 Å, while the bulk modulus increases. The total magnetic moment decreases from 2.00 μ_B (for x = 0.0) to 0.99 μ_B (for x = 1.0). The results of electronic structure show that the alloys with x = 0.0, 0.25, and 0.50 have a half-metallic nature with a real gap in the down-spin band, and 100% spin polarization. For other alloys, the spin polarization decreased with increasing x from 0.75 to 1.0. Although 100% spin polarization was not found for all members of these series, it is quite high value which can be used in industries.

1. Introduction

In the last decades, the physical properties of the half-metallic (HM) materials have been investigated because of their diverse applications in the electronic devices [1-8]. In these materials, an energy gap around the Fermi level (E_F) is observed for one spin band, while for the other band a metallic nature is exhibited. Therefore, they may have 100% spin-polarization (P) [2, 9-12]. This feature makes them excellent candidates for spintronic applications [3, 9, 12, 13]. The spintronic is a swiftly advanced area in the field of modern technology. The main concept of this new technology is to use the spin freedom degree of electrons. Spintronics has the potential advantage of nonvolatility, speeding up of data processing, high circuit integration density, and reduction in power consumption [14]. However, it needs the adequate materials as a source of the spin-polarized charge carriers [15, 16]. For these purposes, the charge carriers injection into a semiconductor, the conventional ferromagnetic metals are not suitable because of low spin polarization. But with the aid of magnetic semiconductors, a high spin polarization of the injected charge carriers has been shown. On the other hand, these require bias fields because they are not spontaneous magnets which make them unsuitable for a variety of applications. For polarized charge-carrier sources, half-metallic systems such as the Heusler alloys are an obvious choice [1, 13, 14, 16, 17]. These alloys are utilized as the magnetic electrodes for using in the giant magneto-resistance (GMR), magnetic sensors, and tunnel magneto-resistance (TMR) devices [5, 18-20]. Among HMs, the Heusler alloys, with high P and Curie temperature (T_C) are favorable [21-23]. In some of these materials, a new ferromagnetic shape-memory behavior has been found which motivated to explore the new alloys from this category [5, 24]. The Heusler alloys can be manufactured using a variety of methods such as the mechanical alloying, arc melting, induction melting, sputtering, and electrodeposition. However, these methods have several challenges such as the contamination problem, high fabrication cost, chemical composition inhomogeneity,

* Corresponding author. Tel.: +98-915-3612994
E-mail address: smojtaba.alavisadr@gmail.com

Cite this article as:

Alavisadr (Zareii) S.M., 2025. Structural, Electronic, and Magnetic Properties of $Mn_2NbAl_{1-x}Si_x$ (x=0.0–1.0) Alloys. *Progress in Physics of Applied Materials*, *5*(2), pp.73-82. DOI: 10.22075/PPAM.2025.36858.1133

time consumption, and susceptibility to oxidation [1, 3, 19]. Accordingly, the theoretical study on Heusler alloys has become widely important due to the difficulties involved in synthesizing and producing these materials. In fact, theoretical investigation is essential for understanding the properties and feasibility of synthesis. The researches emphasize that predicting the physical, magnetic, and electronic properties of Heusler alloys theoretically can lead to the targeted design of compounds that are difficult to synthesize in practice or require the precise control of processing conditions [1, 3, 14, 25].

Among the Heusler alloys, the ferrimagnetic alloys are more favorable than the ferromagnetic ones because of their internal spin compensation and low magnetization, while T_C remains fairly high [9, 26]. Therefore, the external magnetic fields have less effect on these materials as they can be favorable for spintronic applications [3, 9, 27, 28]. Having high T_C guarantees the good thermal stability in these materials [9]. In the Heusler alloys, T_C is much higher than that in other HMs [26]. These alloys are classified as half (XYZ), full (X_2YZ), and quaternary (XX'YZ), where X, X', and Y are transition metals and Z is a sp element [16, 21, 22]. The X_2YZ alloys crystallize either in $AlCu_2Mn$-type (normal) or in $CuHg_2Ti$-type (inverse) structure [29] with atomic positions of A=(0,0,0), B=(0.25,0.25,0.25), C=(0.5,0.5,0.5), and D=(0.75,0.75,075) [30]. In the normal structure, the position of X atom is A and C sites, Y atom is B, and Z atom is D. For inverse structure, X atom occupied A and B sites, while Y and Z atoms occupied C and D, respectively [31]. Slater and Pauling [32, 33] have observed that the magnetic moment of these alloys can be determined according to average valence electron number per atom. As will be discussed later, the Slater–Pauling (SP) rule relates the number of valence electrons to the spin magnetic moment [28, 34]. With substitution of different elements, the functional materials with desirable magnetic properties can be achieved. After the Co-based compounds, Mn_2YZ alloys are the second family that contains many half-metallics (HM). However, it is less studied compared with the first family [35]. The Mn-based alloys have considerable applications in the spintronic, magnetic refrigerators and energy technology [36].

The Mn-based alloys have low magnetic moment which is desirable for using in the spintronic and transfer torque-based devices [27, 36, 37]. The first ferromagnet HM of this family was Mn_2VAl [38]. Later, other Mn-based alloys such as Mn_2VZ (Z = Sn, Ge, Si, In, Ga, Al) [26], Mn_2CrZ (Z = Sb, Ge, Si, Ga, Al) [39], Mn_2CuZ (Z = Al, Ge) [40, 41], Mn_2TiZ (Z = Sb, As, P, Sn, Ge, Si, In, Ga, Al) [9, 15], Mn_2CuSi [42], and Mn_2ZnZ (Z = Ge, Si) [18, 43] were investigated. Jum'h et al. [35] also reported the HF behavior in Mn_2VAl and Mn_2CrAl Heusler compounds. Based on these results, in the Mn_2-based Heusler alloys, the half-metallic ferrimagnet behavior can be observed [1, 17, 35].

However, more investigations are done on the 3d transition metals and fewer researches are concentrated on the 4d transition metal [5, 28]. In this regard, Abada et al. [5] predicted of new Mn_2-based full Heusler alloys Mn_2ZrSi and Mn_2ZrGe by first-principle calculations. Their study indicated that these alloys can be used as promising magnetic materials in spintronic applications. In our previous works [20, 21, 36], we reported the HF characteristics in Mn_2ZrGa compound and for the first time in $Mn_2ZrGa_{1-x}As_x$ (for x=0.5 and 0.75) and $Mn_2ZrGa_{1-x}Ge_x$ (for x=0.75 and 1.0) systems by first-principle calculations. Based on the results reported in [22, 44, 45], the Mn_2RuZ (Z= Si, Ga, Ge) and Mn_2RhZ (Z = Si, Ge, Sn) alloys can also be potential candidates for the spintronic. Ghosh et al. [46] studied Mn_2YAl (Y=Zr, Nb, Mo) by the Pseudo-potential method and concluded that only the Mn_2NbAl compound shows HF behavior. However, their research lacked the analysis of the band structure. In another research, Saber et al. [6] concluded that the Nb-d sates can create or regulate the half-metallic characteristics in the Ru_2NbMn Heusler compounds. However, to our best knowledge, there are few papers that investigate the Mn-based full-Heusler compounds which contain Nb atoms. In this regard, Piyasin et al. [47] indicated that the Heusler compounds containing Mn and Nb can be suitable for thermoelectric and spintronic applications. Kervan et al. [48] observed the HM behavior in Mn_2NbAl alloy by using the first-principles calculations. Sofi et al. [49] studied newly Mn-based Heuslers Mn_2NbX (X=Al, Ga, In) by ab-initio calculations within GGA and mBJ approximations. Their results indicated that the Mn_2NbX alloys are vital applicants for thermoelectric effects, spintronic, power generation, and green energy sources for future technologies. However, there is a shortcoming in their research, and that is the failure to consider the Hubbard parameter U. In fact, the transition metal d electrons are generally strongly correlated and cannot be adequately described within the GGA approximation, because of not including the on-site Coulomb interaction [2, 50]. This limitation of standard DFT can be taken care of by introducing the Hubbard parameter U (DFT+U scheme). The Hubbard parameter consists of the on-site Coulomb interaction parameter U and the exchange interaction parameter J [50]. Accordingly, in the present study, we used the DFT+U scheme. Moreover, the half-metallic ferrimagnet with low total magnetic moment would reduce the energy losses in spintronic devices because the devices would be less affected by the external magnetic field due to its low magnetic strain [12, 37].

The half-metallic ferromagnet with high total magnetic moment would also hinder the spintronic device performance since the external magnetic field would strongly affect the devices due to its large dipole field [51]. The conducted studies on these alloys indicate the energy gap (E_g) usually increases with the lattice volume contraction [11, 34]. The Al substitution by Si in the Mn_2NbAl is expected to affect the magnetic and HM properties of parent alloy, because of the smaller atomic radius of Si and one more valence electron. Si is a semiconductor and its resistance is much higher than Al. Therefore, its substitution can reduce the Eddy currents and energy losses for use in the electronic devices. With these mindsets in this research, the effect of Si substitutions on the physical properties of $Mn_2NbAl_{1-x}Si_x$ (x= 0.0-1.0) are theoretically investigated. In the following, the organization of our work is: Section 2 describes the method of calculations. Section 3 surveys the results and their Interpretation, and Section 4 states a summary of results.

2. Computational Method

The first-principles calculations for simulation of the $Mn_2NbAl_{1-x}Si_x$ alloys were done by the density functional theory (DFT) via the WIEN2k code [52, 53]. Fig.1 illustrates the unit cell of the supercells which were used for the simulation of $Mn_2NbAl_{1-x}Si_x$ alloys. The muffin-tin (MT) sphere radii for the Mn, Nb, Al, and Si atoms were respectively set to 2.25, 2.20, 2.10, and 2.10 a.u. The valence and core states were separated by cut-off energy of -6.5 Ry. These values were chosen such that, while preventing the overlap between the MT spheres, the charge leakage outside these spheres was minimized. The cut-off parameters $R_{MT}\times K_{max}$, l_{max}, and G_{max} were set to 8, 10 and 14 respectively. Moreover, In the irreducible Brillion zone, 120 k-points were used by the Monkorst-Pack method [54]. These values were optimized separately using the energy convergence criterion. In this method, a graph of the changes in total energy of the lattice is plotted versus the changes of that quantity until further increases in the quantity result in no significant energy changes. The generalized gradient approximation with considering the Hubbard term (GGA+U) was selected as the exchange–correlation energy [50]. The value of the Hubbard parameter (U_{eff}) of Mn-3d states in Mn_2NbAl alloy was calculated using the method presented by Madsen et al.[55] and was found to be of about 4.12 eV. The same amount was also used for other alloys in this series (x=0.25-1.0). The spin–orbit coupling is neglected, but it may have strong influence on the spin polarization when the Z atom is a heavy element such as Sn or Sb [9, 11, 28]. The convergence criterion for the self-consistent cycles was 10^{-5} Ry and 10^{-4} electrons simultaneously.

3. Results and Discussion

3.1. Structural Properties

Fig.2 illustrates the calculated total energy E of the $Mn_2NbAl_{1-x}Si_x$ alloys with x=0.0 and 1.0 versus the cell volume V. The calculations were done for the anti-ferromagnetic (AFM), ferromagnetic (FM), and non-magnetic (NM) configurations in both type-structures, i.e. $CuHg_2Ti$ (inverse) and $AlCu_2Mn$ (normal). The obtained data then have fitted with Murnaghan equation of state [56] to obtain the equilibrium ground state parameters such as the lattice parameter, volume, bulk modulus and total energy (Table 1). As seen, the normal structure is thermodynamically more stable than the inverse structure.

Moreover, the total energy of FM states is more negative than that of AFM and NM states. Therefore, the FM states of normal structure of $Mn_2NbAl_{1-x}Si_x$ alloy can be considered as ground state. A similar trend was also observed for the alloys with x = 0.25, 0.5, and 0.75 which is not presented here. The following calculations for the $Mn_2NbAl_{1-x}Si_x$ alloys are only done for the FM state of $AlCu_2Mn$-type structure. Table 1 presents some calculated structural parameters of $Mn_2NbAl_{1-x}Si_x$ alloys in FM equilibrium state for $AlCu_2Mn$-type structure. The accessible measured data by others are also presented for comparison. Moreover, the energy difference between NM and FM configurations ($\Delta E=E_{FM}-E_{NM}$) is calculated for the $AlCu_2Mn$-type structure. As concluded, the calculated lattice constant for Mn_2NbAl (x=0.0) is about 6.01 Å, which is in good agreement with the results of others [46, 48, 49].

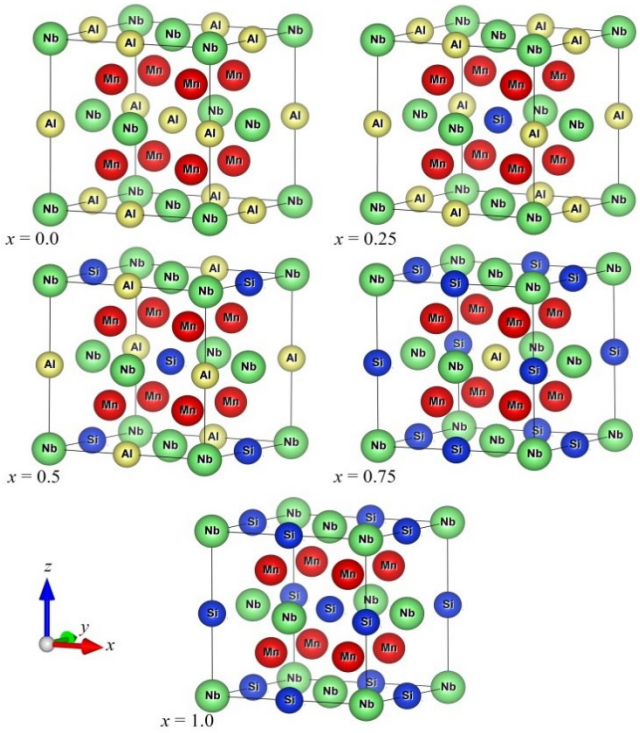

Fig. 1. The unit cells of the calculated supercells for simulation of $Mn_2NbAl_{1-x}Si_x$ alloys

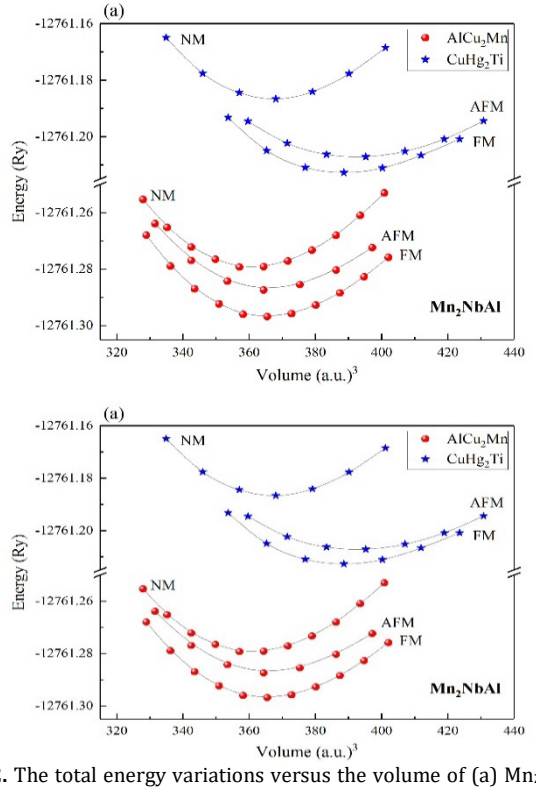

Fig. 2. The total energy variations versus the volume of (a) Mn_2NbAl (x=0) and (b) Mn_2NbSi (x=1.0) for AFM, FM, and NM states of the $CuHg_2Ti$ and $AlCu_2Mn$-type structures

The percentage error for the calculation of this parameter relative to the other measured values is 0.17. For other *x*-values, no other research results are available. However, by comparing the lattice constant of closely related alloys (Table1), it can be concluded that the obtained values can be reasonable. Moreover, as seen from Fig.3, the lattice constant shows a systematic behavior with changes in *x*, as with increment of *x*, it decreases linearly in agreement with Vegard's law. This behavior can be due to the larger atomic radius of Al atom than Si atom as was also observed in our previous work [11] for $Co_2TiAl_{1-x}Si_x$ Heusler alloys. Since the equilibrium lattice constants of the understudied alloys are close to that of zinc blende semiconductors such as InAs (6.058 Å), CdSe (6.077 Å), and ZnTe (6.088 Å)[5], it is suggested to experimentally realize these Heusler alloys in the form of thin films on appropriate substrates and to use them as new candidates for applications in the spintronic field.

However, the bulk modulus *B* increases as *x* increases. In fact, *B* is a measure of the substance's resistance to uniform compression and represents the resistance to fracture [35, 57]. This means that the Mn_2NbAl is more compressible compared to Mn_2NbSi. This behavior is in agreement with the well-known relationship between B and the lattice constant: $B \propto \frac{1}{V}$ ($V=a^3$ is the unit-cell volume) as *V* decreases with increasing *x* [20]. The increase in *B* can also be attributed to the increase in strength of the atomic bonds due to the lattice contraction [7, 8].

Table 1. Comparison of the structural parameters and some physical findings of $Mn_2NbAl_{1-x}Si_x$ alloys with the reported values

Alloy	*a* (Å)	*B* (GPa)	E_f(eV)	E_c(eV)	ΔE (eV)	Ref.
Mn_2NbAl	6.01	196	-1.31	-19.18	0.24	This work
Mn_2NbAl	6.00, 6.01, 6.00	203, 220	-1.37, -1.56	-29.59		[49], [48], [46]
$Mn_2NbAl_{0.75}Si_{0.25}$	5.97	202	-1.39	-19.53	0.17	This work
$Mn_2NbAl_{0.5}Si_{0.5}$	5.94	211	-1.48	-19.89	0.12	This work
$Mn_2NbAl_{0.25}Si_{0.75}$	5.91	216	-1.60	-20.27	0.07	This work
Mn_2NbSi	5.88	227	-1.73	-20.67	0.04	This work
Mn_2VAl	5.81	188		-17.72		[35]
Mn_2MoAl	5.90		-1.23			[46]
Mn_2ZrAl	6.15		-2.01			[46]
Mn_2ZrGa	6.15	150	-0.92			Our previous work [21]
Mn_2ZrGe	6.10	176	-0.97			Our previous work [36]
Mn_2ZrAs	6.06	185	-2.88			Our previous work [20]
Mn_2TiAl, Mn_2TiSi	5.96, 5.82*					[9], [15]
Mn_2RuGa, Mn_2RuGe	6.00*, 5.92*					[44]

* Denotes the accessible experimental data

This is consistent with the increase in the magnitude of the calculated cohesive energy as *x* increases (Table1). Table1 presents the formation (E_f) and cohesive (E_c) energies of $Mn_2NbAl_{1-x}Si_x$ alloys defined by the following equations:

$$E_f = E^{tot}_{Mn_2NbAl_{1-x}Si_x} - \left[2E^{bulk}_{Mn} + E^{bulk}_{Nb} + (1-x)E^{bulk}_{Al} + xE^{bulk}_{Si}\right] \quad (1)$$

$$E_c = E^{tot}_{Mn_2NbAl_{1-x}Si_x} - \left[2E^{iso}_{Mn} + E^{iso}_{Nb} + (1-x)E^{iso}_{Al} + xE^{iso}_{Si}\right] \quad (2)$$

where $E^{tot}_{Mn_2NbAl_{1-x}Si_x}$ is the total energy of the $Mn_2NbAl_{1-x}Si_x$ alloy for formula unit, E^{bulk}_{Mn}, E^{bulk}_{Nb}, E^{bulk}_{Al}, and E^{bulk}_{Si} are the total energies for one atom of Mn, Nb, Al, and Si respectively. Similarly, E^{iso}_{Mn}, E^{iso}_{Nb}, E^{iso}_{Al}, and E^{iso}_{Si} correspond to the energies of the isolated Mn, Nb, Al, and Si atoms. The calculated negative values for E_f and E_c indicate that understudy alloys are stable from the thermodynamic point of view. Moreover, with increasing the Si content, the magnitude of E_f and E_c increases which indicates that the Si-rich alloys have more stable structures. As *x* increases, the energy difference ΔE of $Mn_2NbAl_{1-x}Si_x$ alloys decreases possibly due to a reduction in the magnetic energy contribution as the total magnetic moment decreases (see section 3.3).

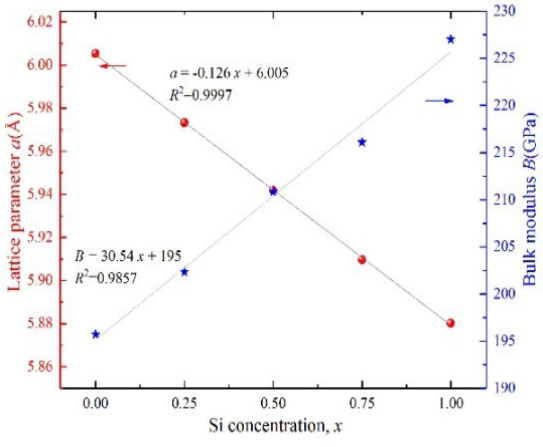

Fig. 3. The variation of the lattice constant *a*, and the bulk modulus *B* of $Mn_2NbAl_{1-x}Si_x$ versus Si concentration

3.2. Electronic Properties

The electronic structure is a key factor in predicting the HM nature and their magnetic properties of the materials [11, 43, 58]. Accordingly, the electronic structure calculations can be useful.

Fig.4 shows the total (TDOS) contribution of density of states $Mn_2NbAl_{1-x}Si_x$ alloys at their equilibrium structure ($AlCu_2Mn$-type) and the partial density of states (PDOS) contribution of their constituent atoms. The zero energy values were devoted to E_F. As seen, for x=0, 0.25 and 0.5 samples, a metallic characteristic is seen for all up-spin bands, while the down-spin bands have a semiconducting gap.

From the contribution of TDOS for the spin-up and spin-down at E_F, i.e. $\rho_\uparrow(E_F)$ and $\rho_\downarrow(E_F)$, the spin-polarization P was calculated from [17]:

$$P = \left| \frac{\rho_\uparrow(E_F) - \rho_\downarrow(E_F)}{\rho_\uparrow(E_F) + \rho_\downarrow(E_F)} \right| \quad (3)$$

The calculated values for P are 100% for x=0, 0.25, and 0.5, and 98% and 95% for x=0.75 and 1.0 respectively. These calculated values are high enough to be useful for practical applications of this alloy in spintronic devices [44].

The high spin polarization is one of the main design criteria for materials and equipment in this emerging technology and influences the efficiency, speed, and stability of these devices [59]. In spin sensors or filters with fully spin-polarized current, the output current is only spin-up or spin-down electrons and hence the output signal and switching efficiency are improved. High spin polarization also reduces the probability of spin scattering and reversal during the transmission path, providing greater stability to spin information [59-61]. Accordingly, the samples with x=0.0, 0.25, and 0.50 can be more suitable for practical applications due to 100% spin polarization. For both spin channels, the TDOS around E_F is mainly originated from the Mn-d and Nb-d states which extend from occupied and unoccupied states. These widely spread d states hybridize with each other as the energy gap around E_F originates predominantly from this hybridization [43].

As seen, in the energy interval of about -6 to 0 eV, d states of Mn and Nb and then the p states of Al and Si have dominant contributions in TDOS. These states are mixed and hybridized with each other, as the strength of the hybridization determines the energy gap width [27]. These mixed states are separated from the next bands which are highly localized within -6 to -10 eV originated from Si-s and Al-s states. In TDOS, the majority and minority spin states are spin-up and spin-down electrons. Therefore, the magnetic moment of these alloys is predicted to be positive (see section 3.3).

On the other hand, since each Si atom has one valence electron more than the Al atom, with increasing Si content, the majority states shift slightly towards more negative energies as the accessible states of spin-up band can be occupied by these extra electrons.

To reveal the role of the type of crystal lattice structure, TDOS was also studied for the $CuHg_2Ti$-type structure (inverse) of Mn_2NbAl and Mn_2NbSi as presented in Fig. 4f. As seen, for $CuHg_2Ti$ type-structure, the shape of TDOS is different compared to that of $AlCu_2Mn$-type structure. The TDOS for the $CuHg_2Ti$-type structure has metallic nature as E_F crosses the up and down-spin bands. For this case, the spin polarization of about 70% and 13% is calculated for Mn_2NbAl and Mn_2NbSi alloys respectively.

Similar behaviors were also observed for TDOS of $CuHg_2Ti$-type structure of the alloys with x=0.25, 0.5, and 0.75, which are not presented here. Therefore, a change in the atomic positions of the alloy can change its electronic structure.

Fig. 5 displays the spin-up energy bands of $AlCu_2Mn$-type structure for $Mn_2NbAl_{1-x}Si_x$ alloys at equilibrium geometry. As seen, for the samples x = 0.75 and 1.0, the spin-up bands have metallic characteristic, while for x = 0.0, 0.25, and 0.5 a real band gap about 0.4 eV is observed around E_F. This value is close to the reported values for the compounds Mn_2NbAl (GGA=0.30 eV, mBJ=0.46 eV) and Mn_2VAl (GGA=0.40 eV) [48, 49]. By increasing x from 0.25 to 1.0, the highly localized states are observed in the energy range from -11 to -8.5 eV. From the PDOS plots (Fig. 4), one can conclude that these ones are related to Si-s states. These bands are well separated from the next bands that arise mostly from Al-s and Si-s states. As seen, with increasing x, the width of the bands located in energy range -6 eV to E_F increases, possibly due to the decrease in lattice parameter and increase in hybridization of p-d orbitals.

The Mn-3d and Nb-3d electrons have dominant contribution for these states. For unoccupied states located above E_F, the dominant contributions belong to the d states of the Mn and Nb atoms. The spin-down bands for the whole series show the metallic natures which have not been demonstrated here. Moreover, it was found that band structure results of these alloys are well consistent with the calculated TDOS.

3.3. Magnetic Properties

As mentioned in section 3.1, the FM states of $AlCu_2Mn$-type structure for $Mn_2NbAl_{1-x}Si_x$ alloys were more stable than NM ones. Fig. 6 shows the changes in total magnetic moments per formula unit (M_{tot}) of the $Mn_2NbAl_{1-x}Si_x$ alloys versus the Si concertation. For a better analysis of this behavior, the contribution of the magnetic moment of the constituent atoms is also presented in Table 2. As seen, with the increasing of Si content, M_{tot} decreases in agreement with the SP rule [32, 33]. The SP rule states that for a Heusler alloy, the M_{tot} depends on the total number of valence electrons (N_t): M_{tot} = 24 - N_t. Since N_t is 22 for the Mn_2NbAl alloy (N_t = (7 × 2) + 5 + 3 = 22), M_{tot} = 24 - 22 = 2.0 μ_B is expected by this rule. Similarly, M_{tot} of 1.75, 1.5, 1.25, and 1.0 μ_B is expected for the alloys with x = 0.25, 0.5, 0.75, and 1.0, respectively.

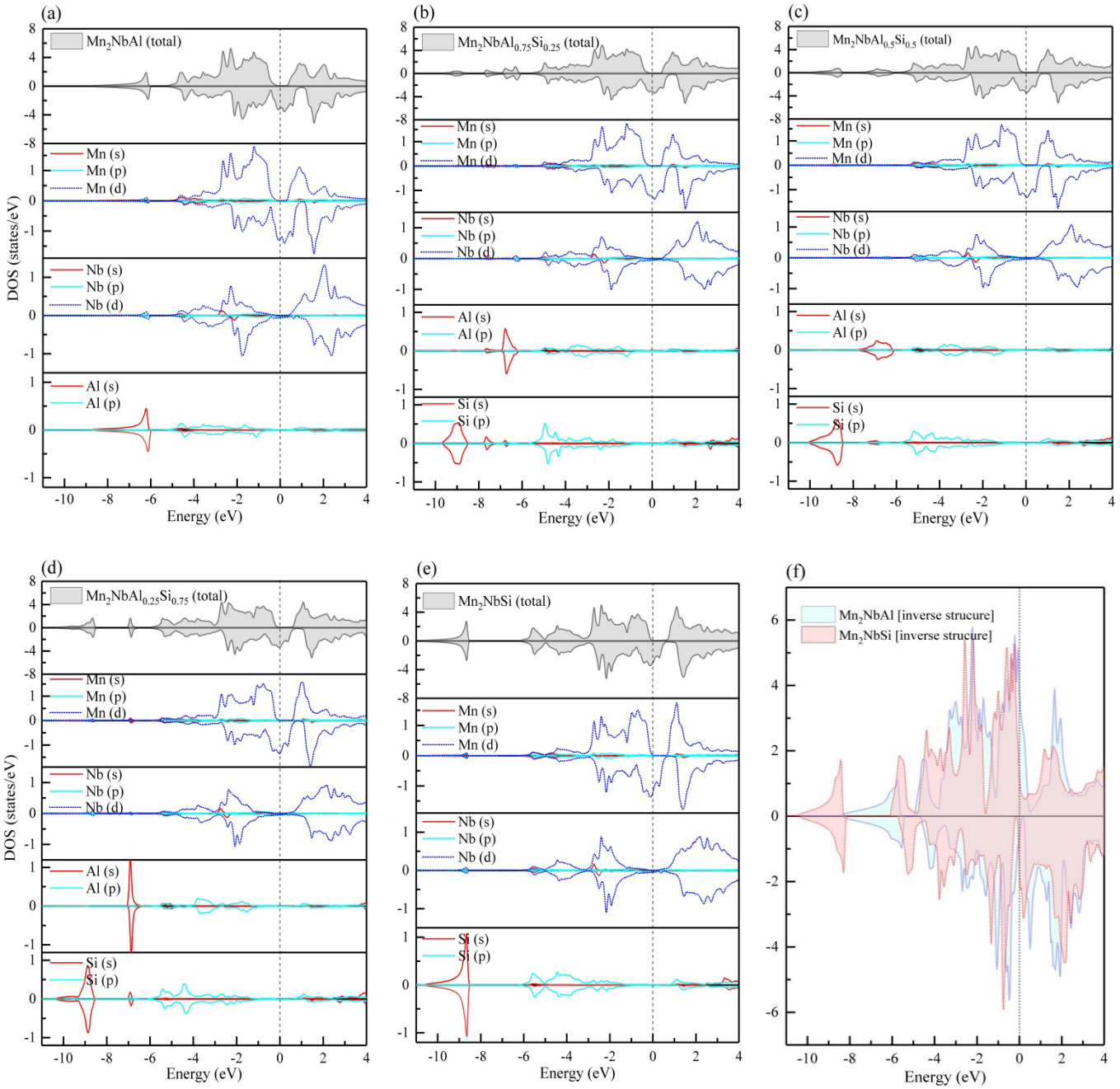

Fig..4. The DOS of $Mn_2NbAl_{1-x}Si_x$ alloys for (a)-(e) $AlCu_2Mn$-type structure, and (f) $CuHg_2Ti$-type structure of Mn_2NbAl and Mn_2NbSi. Positive and negative contributions are devoted to up and down-spin states

This result indicates that only the magnetic moments of the alloys with x = 0.0, 0.25, and 0.50 obey from SP rule. For x = 0.75 and 1.0, the total magnetic moment deviates from SP rule which arises from the existence of a pseudo-gap instead of a real gap around E_F, and the non-zero contribution of spin-up density of states in E_F [20, 62]. This also confirms the stability of HM behavior for x = 0.0, 0.25, and 0.50 as expected from the DOS plots (Fig.4). The Mn atoms have main contribution in M_{tot}, and the other constituent atoms have less influence. In fact, the hybridization of the p states of Al and Si atoms with Mn-3d states induces a small spin polarization on the Al or Si, and hence they get a low magnetic moment. The spin polarization formed in the indirect exchange interaction depends directly on the hybridization between magnetic ions and the delocalized electrons. In other words, the spin of one ion influences the spin of another atom through the hybridization with these electrons [62, 63]. Similarly, Nb atom gets a low magnetic moment due to the hybridization of the d stats of Mn and Nb atoms. Since the direction of the magnetic moments of the Mn atoms is antiparallel to Nb, Al, and Si atoms, the $AlCu_2Mn$-type structure of $Mn_2NbAl_{1-x}Si_x$ alloys is a typical ferrimagnet. But indeed, the magnetic moments of about 2.00, 1.75, 1.50, 1.15, and 0.99 μ_B were calculated for the alloys with x = 0.0, 0.25, 0.5, 0.75, and 1.0 respectively.

Table 2. The total and partial magnetic moments (μ_B) of $Mn_2NbAl_{1-x}Si_x$ alloys. The reported values for closest compounds are also presented for comparison. The accessible experimental data are indicated by *

Alloy (X_2YZ)	Total	Mn (X)	Nb (Y)	Al (Z)	Si (Z)	Ref.
Mn_2NbAl	2.00	1.20	-0.30	-0.03		This work
Mn_2NbAl	2.00	1.19, 1.21, 1.21	-0.39, -0.30, -0.36	-0.03		[49], [48], [46]
$Mn_2NbAl_{0.75}Si_{0.25}$	1.75	1.04	-0.26	-0.02	-0.03	This work
$Mn_2NbAl_{0.5}Si_{0.5}$	1.50	0.92	-0.20	-0.02	-0.03	This work
$Mn_2NbAl_{0.25}Si_{0.75}$	1.15	0.74	-0.18	-0.02	-0.02	This work
Mn_2NbSi	0.99	0.59	-0.14		-0.02	This work
Mn_2Val	1.99	1.40	-0.741 (for V)	-0.0147		[35]
Mn_2ZrAl	3.00	1.73	-0.34 (for Zr)	-0.05 (for Al)		[46]
Mn_2ZrGa	2.99	1.74	-0.27 (for Zr)	-0.05 (for Ga)		Our previous work [21]
Mn_2ZrGe	1.99	1.14	-0.18 (for Zr)	-0.04 (for Ge)		Our previous work [36]
Mn_2ZrAs	0.99	0.59	-0.10 (for Zr)	-0.02 (for As)		Our previous work[20]
Mn_2MoAl	1.04	0.68	-0.31 (for Mo)	-0.01 (for Al)		[46]
Mn_2RuGa, Mn_2RuGe	0.29*, 1.55*					[44]

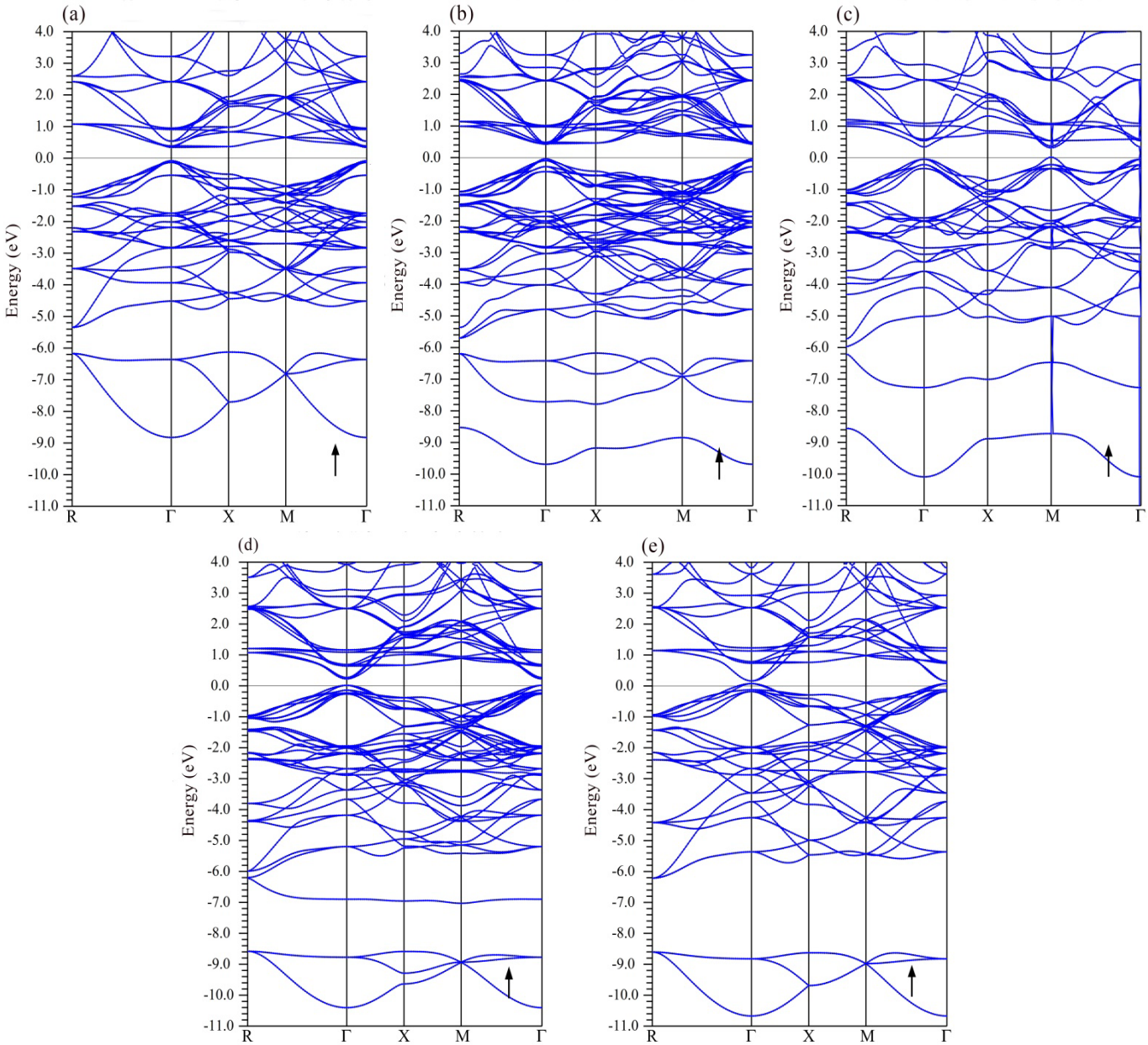

Fig.5. The band structure of spin-up states for (a) x=0, (b) x=0.25, (c) x=0.5, (d) x=0.75, and (e) x=1.0 in $Mn_2NbAl_{1-x}Si_x$ alloys

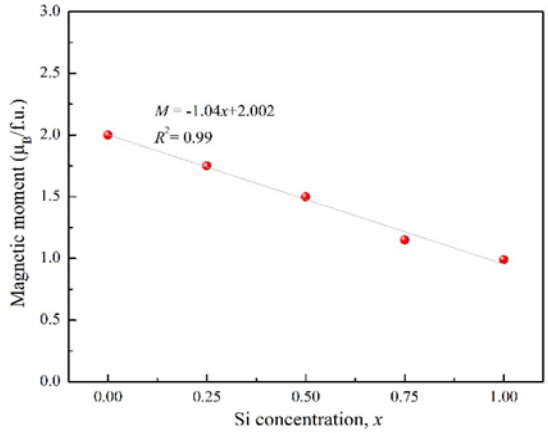

Fig. 6. The variation of total magnetic moment of the $Mn_2NbAl_{1-x}Si_x$ versus Si concentration

4. Conclusions

The structural, electronic, and magnetic properties of $Mn_2NbAl_{1-x}Si_x$ (x=0.0-1.0) alloys were theoretically investigated. For the whole series of this alloy, from x = 0.0 to 1.0, the normal structures are more stable than the inverse ones. Moreover, the complete series $Mn_2NbAl_{1-x}Si_x$ are found to be ferrimagnetic with total magnetic moment which decreases from 2.0 μB to 0.99 μB as x increases. The results of the density of states and band structure show that the alloys with x = 0.0, 0.25, and 0.50 have the HM nature with the spin polarization P=100% and a real energy gap of about 0.4 eV. The results show that the $Mn_2NbAl_{1-x}Si_x$ alloys can be promising materials for using in spintronic industries. The present results can provide some help for future research of Mn_2-based Heusler alloys.

Funding Statement

This research received no specific grant from any funding agency.

Conflicts of interest

The author declares no conflicts of interest.

References

[1] Wederni, A., Daza, J., Ben Mbarek, W., Saurina, J., Escoda, L. and Suñol, J.-J., 2024. Crystal Structure and Properties of Heusler Alloys: A Comprehensive Review. Metals. 14(6), pp. 688.

[2] Chernov, E.D. and Lukoyanov, A.V., 2023. Effect of Electron Correlations on the Electronic Structure and Magnetic Properties of the Full Heusler Alloy Mn2NiAl. Magnetochemistry. 9(7).

[3] Tavares, S., Yang, K. and Meyers, M.A., 2023. Heusler alloys: Past, properties, new alloys, and prospects. Progress in Materials Science. 132, pp. 101017.

[4] Berri, S., 2016. Electronic structure and magnetic properties of Co2TaAl from ab initio calculations. J. Sci.: Adv. Mater. Devices. 1(3), pp. 286-289.

[5] Abada, A., Amara, K., Hiadsi, S. and Amrani, B., 2015. First principles study of a new half-metallic ferrimagnets Mn2-based full Heusler compounds: Mn2ZrSi and Mn2ZrGe. J. Magn. Magn. Mater. 388(0), pp. 59-67.

[6] Saber, N., Fadil, Z., Mhirech, A., Kabouchi, B., Bahmad L. and O., B.W., 2021. Magnetic Properties of the Heusler RuMn (= Nb, Ta or V) Compounds: Monte Carlo Simulations. arXiv. 2109.01708.

[7] Benichou, B., Bouchenafa, H., Nabi, Z. and Bouabdallah, B., 2022. Computational study of structural stability, elastic, electronic, magnetic and thermodynamic properties of the Rh2-based full-Heusler compounds: Rh2MnZ (Z = Sn, Pb, Tl) by FP-LAPW method. Revista Mexicana de Física. 68(6 Nov-Dec), pp. 060502 1-12.

[8] Wu, S.-C., Fecher, G.H., Shahab Naghavi, S. and Felser, C., 2018. Elastic properties and stability of Heusler compounds: Cubic Co2YZ compounds with L21 structure. J. Appl. Phys. 125(8).

[9] Meinert, M., Schmalhorst, J.M. and Reiss, G., 2011. Ab initio prediction of ferrimagnetism, exchange interactions and Curie temperatures in Mn 2 TiZ Heusler compounds. J. Phys.: Condens. Matter. 23(3), pp. 036001.

[10] Felser, C., Wollmann, L., Chadov, S., Fecher, G.H. and Parkin, S.S.P., 2015. Basics and prospective of magnetic Heusler compounds. APL Mater. 3(4), pp. 041518.

[11] Zareii, S.M., Arabi, H. and Sarhaddi, R., 2012. Effect of Si substitution on electronic structure and magnetic properties of Heusler compounds Co2TiAl1−xSix. Physica B. 407(17), pp. 3339-3346.

[12] Liu, L., Hu, L., Liu, S., Xiong, J., Liao, Q. and Wen, Y., 2021. First-principles investigations on the ground-state bulk properties and lattice constant dependent half-metallic ferrimagnetism of MnNbSi full-Heusler compound. International Journal of Quantum Chemistry. 121(7), pp. e26566.

[13] Iram, N., Sharma, R., Ahmed, J., Almeer, R., Kumar, A. and Abbas, Z., 2025. Exploring the physical, magnetic, opto-spintronics and thermoelectric properties of Fe2ZrAs Heusler Alloy through DFT study. Journal of Physics and Chemistry of Solids. 196, pp. 112368.

[14] Hu, X., 2012. Half-Metallic Antiferromagnet as a Prospective Material for Spintronics. Advanced Materials. 24(2), pp. 294-298.

[15] Jayashire, R., Karthik, G., Raja, M.M., Sampath, V. and Ravichandran, K., 2024. Structural and Magnetic Studies on Mn2TiSi Heusler Alloy for Spintronics Applications. J. Supercond. Novel Magn. 37(1), pp. 117-127.

[16] Mohammad Abadi, A.A., Forozani, G., Baizaee, S.M. and Gharaati, A., 2019. Structural, electronic and magnetic properties of CoZrIrSi quaternary Heusler alloy: First-principles study. Journal of Alloys and Compounds, pp. 152449.

[17] Al-Douri, Y. and and Ameri, M., 2025. Physical studies of spintronics-based Heusler alloys. Critical Reviews in Solid State and Materials Sciences. 50(2), pp. 189-238.

[18] Kervan, S. and Kervan, N., 2013. Half-metallic properties of the CuHg2Ti-type Mn2ZnSi full-Heusler compound. Curr. Appl Phys. 13(1), pp. 80-83.

[19] Wenyong, Z., Yunlong, J., Ralph, S., Parashu, K., Xingzhong, L., Tingyong, C., Gejian, Z., Dongrin, K., Shah, V. and David, J.S., 2018. Mn2CrGa-based Heusler alloys with low net moment and high spin polarization. J. Phys. D: Appl. Phys. 51(25), pp. 255001.

[20] Amirabadizadeh, A., Abbas Emami, S.A., Nourbakhsh, Z., Alavi Sadr, S.M. and Baizaee, S.M., 2016. The Effect of Substitution of As for Ga on the Topological Phase and

Structural, Electronic and Magnetic Properties of Mn 2 ZrGa Heusler Alloy. J. Supercond. Novel Magn. 30(4), pp. 1035-1049.

[21] Abbas Emami, S.A., Amirabadizadeh, A., Nourbakhsh, Z., Baizaee, S.M. and Alavi Sadr, S.M., 2018. Study of the Structural, Electronic, Magnetic, and Optical Properties of Mn2ZrGa Full-Heusler Alloy: First-Principles Calculations. J. Supercond. Novel Magn. 31(1), pp. 127-134.

[22] Jiang, D., Ye, Y., Liu, H., Gou, Q., Donglan, W., Wen, Y. and Liu, L., First-principles calculations of electronic, acoustic and anharmonic properties of Mn 2 RuZ (Z = Si and Ge) Heusler compounds. Vol. 458. 2018.

[23] Guermit, Y., Drief, M., Lantri, T., Tagrerout, A., Rached, H., Benkhettou, N.-e. and Rached, D., 2020. Theoretical investigation of magnetic, electronic, thermoelectric and thermodynamic properties of Fe2TaZ (Z= B, In) compounds by GGA and GGA+U approaches. Computational Condensed Matter. 22, pp. e00438.

[24] Shakeel Ahmad, K. and Dinesh, C.G., 2017. DFT investigations on mechanical stability, electronic structure and magnetism in Co 2 TaZ (Z = Al, Ga, In) heusler alloys. Semicond. Sci. Technol. 32(12), pp. 125019.

[25] Gurunani, B., Ghosh, S. and Gupta, D.C., 2024. Comprehensive investigation of half Heusler alloy: Unveiling structural, electronic, magnetic, mechanical, thermodynamic, and transport properties. Intermetallics. 170, pp. 108311.

[26] Özdogan, K., Galanakis, I., Şaşioglu, E. and Aktaş, B., 2006. Search for half-metallic ferrimagnetism in V-based Heusler alloys Mn 2 VZ (Z = Al, Ga, In, Si, Ge, Sn). J. Phys.: Condens. Matter. 18(10), pp. 2905.

[27] Anjami, A., Boochani, A., Elahi, S.M. and Akbari, H., 2017. Ab-initio study of mechanical, half-metallic and optical properties of Mn2ZrX (X=Ge, Si) compounds. Results Phys. 7(Supplement C), pp. 3522-3529.

[28] Skaftouros, S., Özdoğan, K., Şaşıoğlu, E. and Galanakis, I., 2013. Generalized Slater-Pauling rule for the inverse Heusler compounds. Phys. Rev. B: Condens. Matter. 87(2), pp. 024420.

[29] Boumia, L., Dahmane, F., Doumi, B., Rai, D.P., Khandy, S.A., Khachai, H., Meradji, H., Reshak, A.H. and Khenata, R., 2019. Structural, electronic and magnetic properties of new full Heusler alloys Rh2CrZ (Z = Al, Ga, In): First-principles calculations. Chinese Journal of Physics. 59, pp. 281-290.

[30] Alrahamneh, M.J., Khalifeh, J.M. and Mousa, A.A., 2020. Ab-initio calculations of the structural, mechanical, electronic, magnetic and thermoelectric properties of Zr2RhX (X= Ga, In) Heusler alloys. Physica B. 581, pp. 411941.

[31] Kervan, N. and Kervan, S., 2012. A first-principle study of half-metallic ferrimagnetism in the Ti2CoGa Heusler compound. J. Magn. Magn. Mater. 324(4), pp. 645-648.

[32] Slater, J.C., 1936. The Ferromagnetism of Nickel. II. Temperature Effects. Phys. Rev. 49(12), pp. 931-937.

[33] Pauling, L., 1938. The Nature of the Interatomic Forces in Metals. Phys. Rev. 54(11), pp. 899-904.

[34] Semari, F., Dahmane, F., Baki, N., Al-Douri, Y., Akbudak, S., Uğur, G., Uğur, Ş., Bouhemadou, A., Khenata, R. and Voon, C., First-principle calculations of structural, electronic and magnetic investigations of Mn 2 RuGe 1-x Sn x quaternary Heusler alloys. Vol. 56. 2018.

[35] Jum'h, I., essaoud, S., Baaziz, H., Zoulikha, C. and Telfah, A., 2019. Electronic and Magnetic Structure and Elastic and Thermal Properties of Mn2-Based Full Heusler Alloys. J. Supercond. Novel Magn. 32.

[36] Amirabadizadeh, A., Emami, S.A.A., Nourbakhsh, Z., Sadr, S.M.A. and Baizaee, S.M., 2017. The Structural, Electronic, Magnetic, and Optical Properties of Mn2ZrGa1−xGex Heusler Alloys: First-Principles Calculations. J. Supercond. Novel Magn. 31(5), pp. 1515-1525.

[37] Benea, D., Gavrea, R., Coldea, M., Isnard, O. and Pop, V., 2019. Half-metallic compensated ferrimagnetism in the Mn-Co-V-Al Heusler alloys. J. Magn. Magn. Mater. 475, pp. 229-233.

[38] Ishida, S., Asano, S. and Ishida, J., 1984. Bandstructures and Hyperfine Fields of Heusler Alloys. J. Phys. Soc. Jpn. 53(8), pp. 2718-2725.

[39] Luo, H., Zhu, Z., Liu, G., Xu, S., Wu, G., Liu, H., Qu, J. and Li, Y., 2008. Prediction of half-metallic properties for the Heusler alloys Mn2CrZ (Z=Al, Ga, Si, Ge, Sb): A first-principles study. J. Magn. Magn. Mater. 320(3–4), pp. 421-428.

[40] Li, S.T., Ren, Z., Zhang, X.H. and Cao, C.M., 2009. Electronic structure and magnetism of Mn2CuAl: A first-principles study. Physica B. 404(14–15), pp. 1965-1968.

[41] Wei, X.-P., Hu, X.-R., Mao, G.-Y., Chu, S.-B., Lei, T., Hu, L.-B. and Deng, J.-B., 2010. Half-metallic ferrimagnetism in Mn2CuGe. J. Magn. Magn. Mater. 322(20), pp. 3204-3207.

[42] Wei, X.-P., Hu, X.-R., Chu, S.-B., Mao, G.-Y., Hu, L.-B., Lei, T. and Deng, J.-B., 2011. A first principles study on the full-Heusler compound Mn2CuSi. Physica B. 406(5), pp. 1139-1142.

[43] Wei, X.-P., Hu, X.-R., Liu, B., Lei, Y., Deng, H., Yang, M.-K. and Deng, J.-B., 2011. Electronic structure and magnetism in full-Heusler compound Mn2ZnGe. J. Magn. Magn. Mater. 323(12), pp. 1606-1610.

[44] Yang, L., Liu, B., Meng, F., Liu, H., Luo, H., Liu, E., Wang, W. and Wu, G., 2015. Magnetic properties of Heusler alloy Mn2RuGe and Mn2RuGa ribbons. J. Magn. Magn. Mater. 379(0), pp. 1-5.

[45] Bensaid, D., Hellal, T., Ameri, M., Azzaz, Y., Doumi, B., Al-Douri, Y., Abderrahim, B. and Benzoudji, F., 2016. First-Principle Investigation of Structural, Electronic and Magnetic Properties in Mn2RhZ (Z = Si, Ge, and Sn) Heusler Alloys. J. Supercond. Novel Magn. 29(7), pp. 1843-1850.

[46] Ghosh, S. and Ghosh, S., 2019. Systematic understanding of half-metallicity of ternary compounds in Heusler and Inverse Heusler structures with 3d and 4d elements. Physica Scripta. 94(12), pp. 125001.

[47] Piyasin, P., Pinitsoontorn, S., Sauerschnig, P., Imasato, K. and Ohta, M., 2024. Power generation from n-type NbCo1−xNixSn and p-type NbFe1−xMnxSb ternary half-Heusler compounds: from materials development to module fabrication. Journal of Materials Chemistry C. 12(34), pp. 13242-13254.

[48] Kervan, N., Kervan, S., Canko, O., Atiş, M. and Taşkın, F., 2016. Half-Metallic Ferrimagnetism in the Mn2NbAl Full-Heusler Compound: a First-Principles Study. J. Supercond. Novel Magn. 29(1), pp. 187-192.

[49] Sofi, S. and Gupta, D., 2020. Investigation of structural, elastic, thermophysical, magneto-electronic and transport properties of newly tailored Mn-based Heuslers: A DFT Study. International Journal of Quantum Chemistry. 120.

[50] Anisimov, V.I., Aryasetiawan, F. and Lichtenstein, A.I., 1997. First-principles calculations of the electronic structure and spectra of strongly correlated systems: the LDA+U

method. Journal of Physics: Condensed Matter. 9(4), pp. 767-808.
[51] Stinshoff, R., Nayak, A.K., Fecher, G.H., Balke, B., Ouardi, S., Skourski, Y., Nakamura, T. and Felser, C., 2017. Completely compensated ferrimagnetism and sublattice spin crossing in the half-metallic Heusler compound Phys. Rev. B: Condens. Matter. 95(6), pp. 060410.
[52] Schwarz, K., Blaha, P. and Madsen, G.K.H., 2002. Electronic structure calculations of solids using the WIEN2k package for material sciences. Comput. Phys. Commun. 147(1), pp. 71-76.
[53] Schwarz, K. and Blaha, P., 2003. Solid state calculations using WIEN2k. Computational Materials Science. 28(2), pp. 259-273.
[54] Monkhorst, H.J. and Pack, J.D., 1976. Special points for Brillouin-zone integrations. Phys. Rev. B: Condens. Matter. 13(12), pp. 5188-5192.
[55] Madsen, G.K.H. and Novák, P., 2005. Charge order in magnetite. An LDA+U study. Europhysics Letters. 69(5), pp. 777.
[56] Murnaghan, F.D., 1944. The Compressibility of Media under Extreme Pressures. Proceedings of the National Academy of Sciences of the United States of America. 30(9), pp. 244-247.
[57] Sharma, S. and Kumar, P., 2017. Investigation of electronic, magnetic and transport properties of full-Heusler alloys Fe2TiX (X = As and Sb). Chinese Journal of Physics. 55(5), pp. 1972-1980.
[58] Hem, C.K., Gerhard, H.F. and Claudia, F., 2007. Calculated electronic and magnetic properties of the half-metallic, transition metal based Heusler compounds. J. Phys. D: Appl. Phys. 40(6), pp. 1507.
[59] Žutić, I., Fabian, J. and Sarma, S.D., 2004. Spintronics: Fundamentals and applications. Reviews of modern physics. 76(2), pp. 323.
[60] Eschrig, M., 2011. Spin-polarized supercurrents for spintronics. Physics Today. 64(1), pp. 43-49.
[61] Inomata, K., Naomichi, I., Nobuki, T., Ryogo, G., Satoshi, S., Marek, W. and and Jedryka, E., 2008. Highly spin-polarized materials and devices for spintronics∗. Science and Technology of Advanced Materials. 9(1), pp. 014101.
[62] Wurmehl, S., Fecher, G.H., Kandpal, H.C., Ksenofontov, V., Felser, C., Lin, H.-J. and Morais, J., 2005. Geometric, electronic, and magnetic structure of Co2FeSi: Curie temperature and magnetic moment measurements and calculations. Phys. Rev. B: Condens. Matter. 72(18), pp. 184434.
[63] Kübler, J., William, A.R. and Sommers, C.B., 1983. Formation and coupling of magnetic moments in Heusler alloys. Phys. Rev. B: Condens. Matter. 28(4), pp. 1745-1755.